

## Article

# Multi-Genotype Rice Yield Prediction Based on Time-Series Remote Sensing Images and Dynamic Process Clustering

Qian Li <sup>1</sup>, Shaoshuai Zhao <sup>1</sup>, Lei Du <sup>1</sup> and Shanjun Luo <sup>1,2,\*</sup> 

<sup>1</sup> Aerospace Information Research Institute, Henan Academy of Sciences, Zhengzhou 450046, China; liqian@hnas.ac.cn (Q.L.); zss@hnas.ac.cn (S.Z.); dulei@hnas.ac.cn (L.D.)

<sup>2</sup> School of Remote Sensing and Information Engineering, Wuhan University, Wuhan 430079, China

\* Correspondence: luoshanjun@hnas.ac.cn

**Abstract:** Predicting rice yield in a timely, precise, and efficient manner is crucial for directing agricultural output and creating food policy. The goal of this work was to create a stable, high-precision estimate model for the yield prediction of multi-genotype rice combined with dynamic growth processes. By obtaining RGB and multispectral data of the rice canopy during the whole development stage, several bands of reflectance, vegetation index, canopy height, and canopy volume were retrieved. These remote sensing properties were used to define several curves of the rice-growing process. The k-shape technique was utilized to cluster the various characteristics based on rice growth features, and data from different groups were subsequently employed to create a yield estimation model. The results demonstrated that, in comparison to utilizing solely spectral and geometric factors, the accuracy of the multi-genotype rice estimate model based on dynamic process clustering was much higher. With a root mean square error of 315.39 kg/ha and a coefficient of determination of 0.82, the rice yield calculation based on canopy volume temporal characteristics was the most accurate. The proposed approach can support precision agriculture and improve the extraction of characteristics related to the rice growth process.

**Keywords:** yield estimation; vegetation indices; canopy height; canopy volume; UAV; dynamic process clustering



Academic Editor: Yongchao Tian

Received: 14 November 2024

Revised: 26 December 2024

Accepted: 28 December 2024

Published: 29 December 2024

**Citation:** Li, Q.; Zhao, S.; Du, L.; Luo, S. Multi-Genotype Rice Yield Prediction Based on Time-Series Remote Sensing Images and Dynamic Process Clustering. *Agriculture* **2025**, *15*, 64. <https://doi.org/10.3390/agriculture15010064>

**Copyright:** © 2024 by the authors. Licensee MDPI, Basel, Switzerland.

This article is an open access article distributed under the terms and conditions of the Creative Commons Attribution (CC BY) license (<https://creativecommons.org/licenses/by/4.0/>).

## 1. Introduction

Rice serves as a staple diet for almost half of the world's population, particularly in Asia [1]. It is a vital component of everyday nutrition and is high in proteins, carbohydrates, vitamins, and minerals [2]. Rice is a staple crop in many nations, and the state of its development and output has a direct impact on the food security of each nation [3]. In addition to aiding in the development of national food security-related policy decisions, macro-control of grain market prices, and international grain trade, a quick and accurate understanding of pre-harvest yield data is crucial for the precise provision of agricultural insurance and wise management of farmland [4,5]. Predicting rice yield is so crucial for ensuring food security, assisting in agricultural decision-making, advancing science and technology, adjusting to climate change, preserving social stability, and facilitating international commerce.

Crop yield estimation is complicated, lagging, and not feasible on a large scale due to the time-consuming, labor-intensive, and expert knowledge-required nature of traditional methods, which primarily involve field sampling surveys, meteorological forecasts, and agronomical forecasts [6]. Furthermore, conventional on-the-ground manual yield assessment techniques are ineffective and vulnerable to plant damage, making them unsuitable

for yield estimation [7]. As a quick monitoring, analysis, and diagnostic tool that can reliably gather crop image data across large regions, remote sensing is extensively utilized in many facets of smart agriculture [8]. Since the 1970s, optical satellite data with certain properties, like spatial, temporal, and spectral resolution, have been widely employed for large-scale crop production prediction due to advancements in remote sensing technology [9,10]. However, the timeliness of data collection cannot be guaranteed due to the coarse and weather-sensitive geographical and temporal resolutions of satellite data, which have a greater impact on regional agricultural output prediction. In recent years, crop growth monitoring has become more efficient owing to unmanned aerial vehicle (UAV) remote sensing technology, which can flexibly carry various sensors and efficiently capture high spatial and temporal resolution image data [11]. UAV-based remote sensing offers new prospects for remote sensing technologies by monitoring a greater range than ground-based measurement methods, better spatial resolution, more frequent observation opportunities, and lower costs than satellite and airplane observations [12]. Thus, there is much promise for rice yield estimation in the field using UAV remote sensing technologies.

Differentiated field data configurations are used in the majority of current crop remote sensing studies for yield estimation. Most field studies are planned using irrigation, planting techniques, and fertilizer gradient control [13–15]. However, it is challenging to match the experimental design in actual crop field production. This makes it challenging to use current estimating models in real-world field settings. Field managers adequately fertilize the soil before planting. Varieties and planting dates may vary among rice fields grown by different farmers. Producers will manage their acreage in a more sophisticated manner, particularly given China's current cropland fragmentation scenario [16]. Because of this, inconsistent irrigation or fertilizer use is quite uncommon. Therefore, there are few existing studies on remote sensing for yield estimation of data under the natural growing state, which makes it difficult to meet the needs of actual farmland management.

The vegetation index (VI), which is computed using UAV image reflectance, has been shown to be an effective crop yield forecast indicator [17]. The rapid development of UAVs has also enhanced the acquisition frequency and spatial and temporal resolution of crop image data. For instance, Zhou et al. employed a UAV fitted with a digital camera and a multispectral camera to capture images of rice at various stages. They then used multiple linear regression (MLR) to analyze the relationship between different VIs and rice yield. According to the findings, the visible atmospherically resistance index (VARI), which was computed using MLR and digital imagery, performed best during the jointing and booting stages, while the normalized difference vegetation index (NDVI), which was computed using MLR and multispectral imagery, performed best during the booting and heading stages [18]. Furthermore, data, including canopy temperature, height, and texture, have been suggested for crop yield estimation [13,15,19]. However, for rice, canopy changes are very complicated as the reproductive cycle shifts, and it is difficult to provide generalizable indications for yield prediction utilizing the aforementioned indicators. Vegetation indices perform poorly in predicting yield at later stages of crops because it has been argued that yield is the result of the nonlinear accumulation of crop photosynthetic products, and traditional linear regression models are unable to adequately capture this complex nonlinear relationship. As a result, when predicting agricultural yield, researchers choose nonlinear methods like machine learning [19,20]. Machine learning can better handle nonlinear relationships between large amounts of data. However, it is weak in handling complex nonlinear relationships and time-series data and is ineffective in predicting yield for multiple varieties with large variations in morphological structure and growth stage [21]. The performance of machine learning models is affected by a variety of factors, including training data, input variables, crop type, and growth stage. One of the most popular

techniques for estimating yield is linear regression, which frequently works well because of its high interpretability [22].

In recent years, phenology has been shown to provide critical information for crop yield prediction [23]. Studies have indicated that dividing the time window by phenological stage allows for a more accurate extraction of environmental variables to capture the complex interactions between crop growth and external factors [24]. Most current research on crop yield estimation focuses on the use of single-period variables or the integration of multi-period variables [4]. When using single-period variables, the correlation between variables and yield from sowing to maturity is often analyzed, and finally, the variables with high correlation are filtered out for direct yield prediction. When multi-period variables are employed, a matrix of variables from multiple periods is often obtained as inputs for machine learning or multiple regression models for yield estimation. However, information on crop variables in different periods has distinct growth dimensions and cannot be directly compared and integrated. Therefore, determining the phenological period of a crop is essential to guarantee the accuracy of growth monitoring and yield prediction. The threshold, maximum slope, and curve fitting methods of optical remote sensing have been utilized to monitor crop phenology [25]. These approaches can only detect the stage of obvious change in greenness based on inflection points and cannot monitor other key stages closely related to agricultural practices. Moreover, accurate real-time monitoring of phenology can be realized based on remote sensing data and classification algorithms. However, this requires a large amount of known phenological data. The essence of classifying different phenological periods is to distinguish variable features at various stages. This problem can be solved if a suitable division method of variables is found to distinguish their differences. The k-shape clustering algorithm is a typical classification technique based on the changing features of a time series, which has the advantage of dealing with the signals of diverse domains. The basic idea is to calculate the similarity between time series based on the distance of the shape to realize clustering [26]. Remote sensing feature variables are characterized by a time series. Therefore, there is potential for the classification of remote sensing features based on time series.

Two separate experiments that simulated rice cultivation under natural growing conditions were created for this investigation. A UAV remote sensing platform was equipped with both an RGB and a multispectral camera to obtain high-frequency observations of rice throughout its growth stage. The k-shape approach was utilized to accomplish high-precision prediction of multi-genotype (multi-species) rice yield based on temporal growth feature clustering by analyzing the contribution of spectral and structural information to the yield estimation of multi-genotype rice. The specific goals of this study were to (1) compare the effects of geometric and spectral information on multi-genotype rice yield estimation, (2) choose variables that are appropriate for characterizing the features of the rice growth process, and (3) forecast multi-genotype rice yield by clustering growth process features.

## 2. Materials and Methods

### 2.1. Experimental Design

The data used in this investigation came from three field-independent investigations that used multiple rice genotypes and replicated rice cultivation under natural growth conditions, as shown in Figure 1. Different hybrid varieties of rice were cultivated in each of the 289 plots in Experiment 1 (2022, Exp. 1). Each plot had a one-square-meter area. In Experiment 2 (2019, Exp. 2), 48 plots representing 48 distinct rice varieties were planted. Each field plot had a total area of roughly 40 square meters. Except for the various rice genotypes, all field management procedures were the same. The uniform rate of nitrogen fertilizer application was 180 kg/ha. Before transplanting, 50% of the nitrogen fertilizer

was applied as a basal fertilizer, 25% was applied during the tillering stage, and 25% was applied during the booting stage. Phosphorus and potash fertilizers were applied as one-time basal fertilizers at 90 kg/ha and 180 kg/ha, respectively. In Experiment 3 (2022, Exp. 3), three nitrogen gradient levels were set up, N1/4, N1, and N2, representing nitrogen applications of 36.3, 144, and 288 kg/ha. Meanwhile, three replications were set up, and the three varieties were randomized. In total, there were 27 plots with an area of about 15 m<sup>2</sup> each. The management practices remained the same as in Experiments 1 and 2, except for the differences in varieties and N fertilization levels. This study was conducted on a plot scale. Each plot was planted with an individual rice variety.

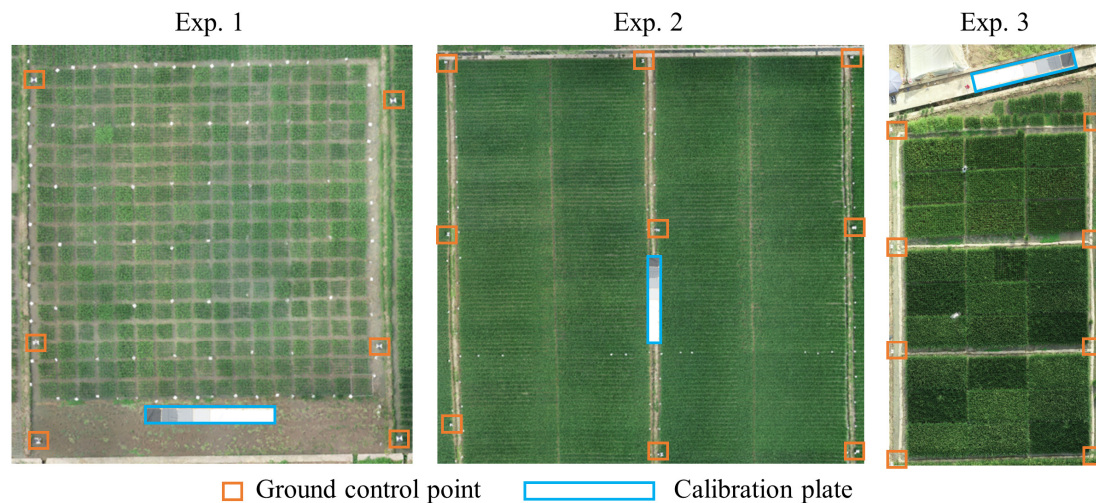


**Figure 1.** Experimental arrangement and plot layout.

## 2.2. Data Acquisition and Processing

### 2.2.1. UAV RGB Image

RGB images of the rice canopy were acquired using a Phantom 4 Pro quadcopter drone manufactured by DJI Innovation (SZ DJI Technology Co., Ltd., Shenzhen, China). The altitude of the UAV was set to 30 m, and the overlap was 90% in heading and 70% in side direction. The average flight speed of the UAV was set to 5 m/s. The data acquisition time required per unit area (1 m<sup>2</sup>) was calculated to be approximately 0.6 s based on the experimental area. The gimbal of the UAV ensured that the camera was always vertically downward during image acquisition. The camera has a field of view of 84°, an image size of 5472 × 3648 pixels, and a ground resolution of about 1 cm/pixel. The aperture size and ISO sensitivity were set before aerial photography according to the actual lighting conditions in the field, and the camera parameters remained unchanged throughout the aerial photography image acquisition process.

After acquiring the RGB images of the experimental area, Agisoft Photoscan Professional software (version 1.4.5, Agisoft LLC, St. Petersburg, Russia) was used for image stitching and 3D reconstruction to generate a dense 3D point cloud, digital elevation model (DEM), digital surface model (DSM), and orthomosaic products of the experimental area based on the coordinates of the ground control points. The Photoscan software is based on the Structure from Motion (SfM) and Multi-View Stereo (MVS) algorithms for image processing. RGB data were collected during 10 periods (denoted as S1–S10), including the tillering, jointing, booting, heading, and ripening stages of rice, with an interval of 5–10 days between each collection.

### 2.2.2. UAV Multispectral Image

An S1000 UAV (S1000, SZ DJI Technology, Co., Ltd., Shenzhen, China) equipped with an MCA series multispectral camera (Tetracam, Inc., Chatsworth, CA, USA) was used to collect the multispectral data. It was clear, cloudless, and windless when the UAV mission was selected. The time frame for gathering the data was consistent from 10:00 to 14:00 local time. A 12-band MCA (center bands: 490, 520, 550, 570, 670, 680, 700, 720, 800, 850, 900, and 950 nm) was the multispectral camera utilized in this investigation. The RGB and multispectral image acquisition times were identical.

The UAV multispectral image processing involves three steps: geometrical processing, radiative handling, and spectral information acquisition. The geometrical processing of UAV multispectral images acquired based on the MCA camera includes halation calibration, waveband registration, and distortion modification, which is accomplished using the MCA image-specific programming tool PixelWrech2 (Tetracam, Inc., Chatsworth, CA, USA). Radiative handling consists mainly of radiometric calibration. In this work, eight calibrators with available known reflectances (3%, 6%, 12%, 24%, 36%, 48%, 56%, and 80%) were used for radiometric calibration, as shown in Figure 1. The radiometric calibration approach was based on the PEL method [23]. Spectral information acquisition comprises region of interest (ROI) outlining and reflectance retrieval.

### 2.2.3. Rice Yield

After the rice of all genotypes had matured, the rice yield was measured in each plot by manual sampling. After manual harvesting, threshing, drying, water content determination, and weighing, the measured rice yield was calculated based on the number of samples taken, weight reading of the samples, transplanting density, and water content.

### 2.3. Vegetation Indices Construction

Vegetation indices have been proposed to reflect dynamic alternation in the full growth cycle of vegetation through the combination of different bands of reflectance. They are related to leaf pigmentation, photosynthesis, and plant nutrient status and are useful for monitoring rice growth. In this study, six vegetation indices that proved to be effective in monitoring vegetation growth and yield prediction were selected, as shown in Table 1.

**Table 1.** The vegetation indices selected in this study.

Vegetation Indices	Formula	Reference
NDVI	$(R850 \text{ nm} - R670 \text{ nm}) / (R850 \text{ nm} + R670 \text{ nm})$	[27]
GNDVI	$(R850 \text{ nm} - R550 \text{ nm}) / (R850 \text{ nm} + R550 \text{ nm})$	[28]
NDRE	$(R850 \text{ nm} - R720 \text{ nm}) / (R850 \text{ nm} + R720 \text{ nm})$	[29]
$CI_{\text{reg\_edge}}$	$R850 \text{ nm} / R720 \text{ nm} - 1$	[30]
EVI2	$2.5 \times (R850 \text{ nm} - R670 \text{ nm}) / (R850 \text{ nm} + 2.4 \times R670 \text{ nm} + 1)$	[31]
$CI_{\text{green}}$	$R850 \text{ nm} / R550 \text{ nm} - 1$	[32]

### 2.4. Rice Canopy Height and Canopy Volume Extraction

To obtain an accurate canopy height (CH) and reduce the effect of ground undulation, the DEM of the base ground was acquired before rice was transplanted to the field. After the seedlings are transplanted, the DSM product generated from each aerial photograph is subtracted from the base ground DEM, which is the rice canopy height model (CHM). On the CHM image, the rice canopy area was selected by outlining the ROIs, and the average value of CH of all pixels in the range of each ROI was computed as the canopy height of the plot. The acquisition process of rice CH is shown in Figure 2.

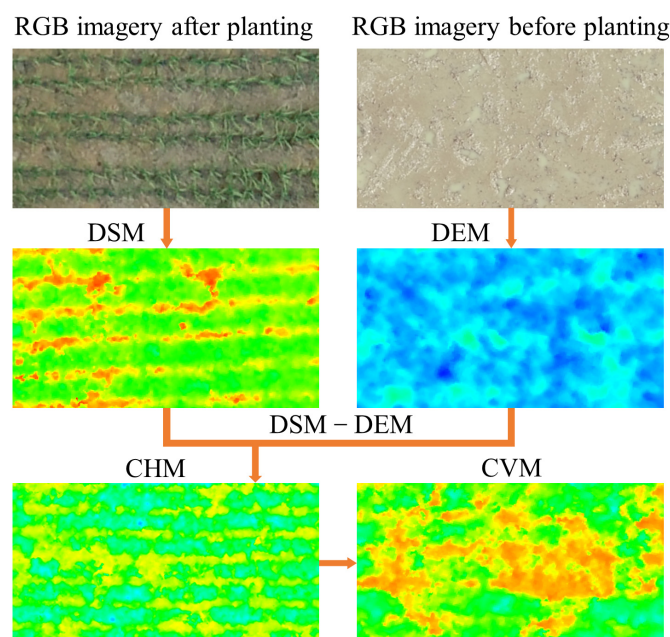


**Figure 2.** Canopy height and canopy volume extraction process.

After obtaining the canopy CHM, the canopy volume model (CVM) can be obtained by combining the ground sampling distance (GSD) information of each pixel. Similar to CH, the CV of each plot can be calculated using the ROI tool. The formula for CV is shown in Equation (1).

$$CV = \sum CH_i \times GSD^2 \quad (1)$$

where  $CH_i$  is the canopy height of the  $i$ th pixel.

### 2.5. K-Shape Clustering Method

An accurate, scalable, and domain-independent time-series clustering approach used in this study is the k-shape algorithm [33]. The program can calculate the distances for shapes and has a distance measure that is independent of movement and scaling. The iterative enhancement mechanism at the core of the algorithm creates homogeneous and better-separated clusters. To update the cluster assignments of the time series in each iteration, a method that the algorithm uses to compute the cluster centers is provided, based on the features of the standard inter-correlation distance measure [26]. The specific steps are as follows: (1) Computation of the mutual correlation function. The mutual correlation function reflects the degree to which the two sequences match each other at different relative positions. (2) Normalization of the correlation function. (3) Calculation of the shape-based distance (SBD). The larger the correlation function, the smaller the SBD. (4) Calculating the mass center of the class based on SBD. (5) Implementation of k-shape clustering. Initially, sequences are randomly assigned to clusters,  $k$  sequences are randomly selected, and the mass center of each cluster is computed. Subsequently, the SBD of each sequence with the mass center of the existing clusters is computed from scratch, and when the SBD is the smallest, it is classified into the cluster, and the mass center of each cluster is updated dynamically. Finally, iterations are performed until the change in the mass center of each cluster is less than a threshold or a specified number of iterations is reached.

### 2.6. Model Evaluation and Technology Roadmap

In this study, a ten-fold cross-validation method was used for accuracy statistics, and the model calibration and validation processes are shown in Figure 3. Ten-fold cross-validation is a widely used method for model evaluation. It divides the dataset into

ten equal parts, and in each iteration, nine of them are taken as the training set and the remaining one as the test set. This is performed in a cycle until each copy of the data is used as a test set. Eventually, the test results of the ten iterations are averaged to obtain an assessment of the model performance. This approach makes full use of the data, reduces the variance in model assessment, and improves the stability and reliability of the assessment results. In Exp. 1, a ten-fold cross-validation method was used. Exp. 2 and Exp. 3 measure the migration ability of the model as independent validation data. The coefficient of determination ( $R^2$ ) and root mean square error (RMSE) were selected for the assessment of rice yield prediction models. The technology roadmap for rice yield prediction in this study is shown in Figure 4.

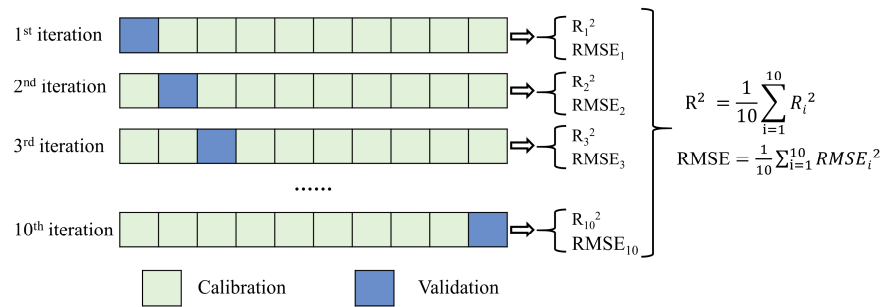


**Figure 3.** Ten-fold cross-validation schematic diagram.

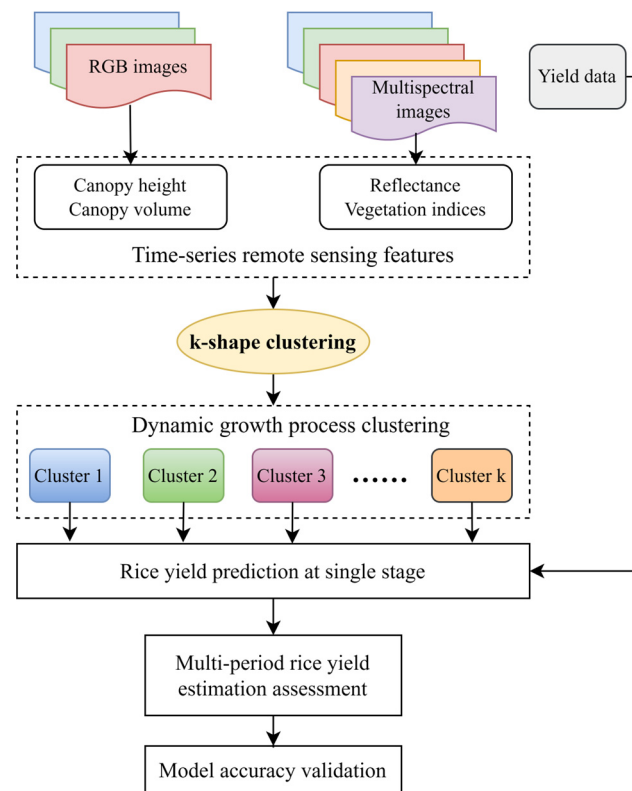


**Figure 4.** Technology roadmap for rice yield estimation.

### 3. Results

#### 3.1. Canopy Height Extraction Results

Due to the time-consuming and labor-intensive measurement of rice canopy height using manual methods, the timely acquisition of real data for a large number of samples could not be accomplished. Taking Exp. 1 as an example, the actual canopy heights of different parts of the samples were measured in ten periods, and 765 sample data were

finally obtained. UAV remote sensing technology was used to obtain the rice canopy height of the corresponding actual measured plots, and the comparison results are shown in Figure 5. It can be seen that the rice canopy height obtained by UAV remote sensing technology has a very high precision, with an overall RMSE of 0.04 m. All sample points are distributed near the 1:1 line. Therefore, the rice CH obtained by remote sensing methods can replace the measured data. The UAV-acquired CH was used for all calculations in the subsequent modeling process.

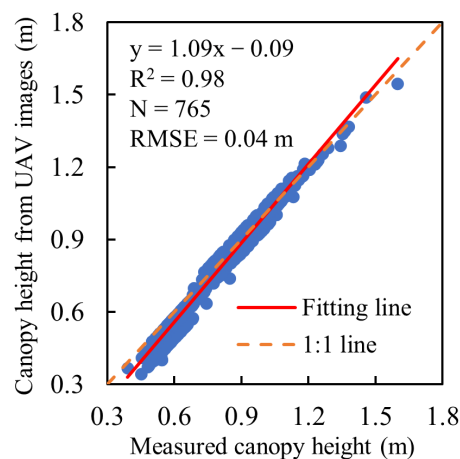


**Figure 5.** Comparison of rice canopy heights acquired from UAV RGB images with measured values.

### 3.2. Rice Yield Prediction Based on VIs, CH, and CV

Before predicting rice yield, it is necessary to analyze the changes in each predictor variable over time. The 720 nm band reflectance, NDRE,  $CI_{green}$ , and CH of some plots were taken as an example to be analyzed, and the results are shown in Figure 6. It can be seen that the variations in red-edge band reflectance with time show a general trend of gradual increase. However, there is obvious volatility. NDRE showed an overall trend of first increasing, then remaining relatively stable, and finally decreasing over time. Compared to reflectance, volatility is weakened.  $CI_{green}$  shows a consistent trend with NDRE overall, but there is spurious volatility. Compared to red-edge reflectance, NDRE, and  $CI_{green}$ , CH exhibits the weakest volatility, showing an overall trend of increasing and then stabilizing. It is worth noting that there is an apparent commonality in the selected indicators, i.e., there are several samples with a consistent trend in volatility but with a large difference in trend from the others. In the case of the NDRE, for example, it is clear that some samples show a curve of dramatic growth, followed by stabilization, and finally a sharp decline. Another class of samples exists that shows a stable and constant curve, followed by a gradual increase, and finally, a decrease in volatility. Moreover, in the middle stage of the growth stage, the indicators show more complex patterns of change, especially the red-edge band reflectance and  $CI_{green}$ . The overall pattern of change in these variables can be divided into more similar combinations of samples.

The correlation of the six vegetation indices, CH and CV, constructed in this study, with the final yield at different stages was analyzed, and the results are shown in Figure 7. In the correlation heatmap, darker colors indicate higher Pearson correlation coefficients. \* indicates a significant correlation at a 0.05 confidence level. In terms of individual periods, almost all remotely sensed variables showed an insignificant correlation with yield, except for EVI2 in period S3. In cases where multiple period variables jointly predicted rice yield, multiple linear regression methods were used to fuse variables from different stages. It can be seen that all the variables were significantly correlated with rice yield except NDVI, GNDVI, and  $CI_{green}$ . Among these, NDRE, CH, and CV showed the strongest correlations.

This indicates that multi-period remote sensing data have the potential to improve the accuracy of rice yield prediction. However, the correlation coefficients are still below 0.6, and further accuracy improvement is needed.

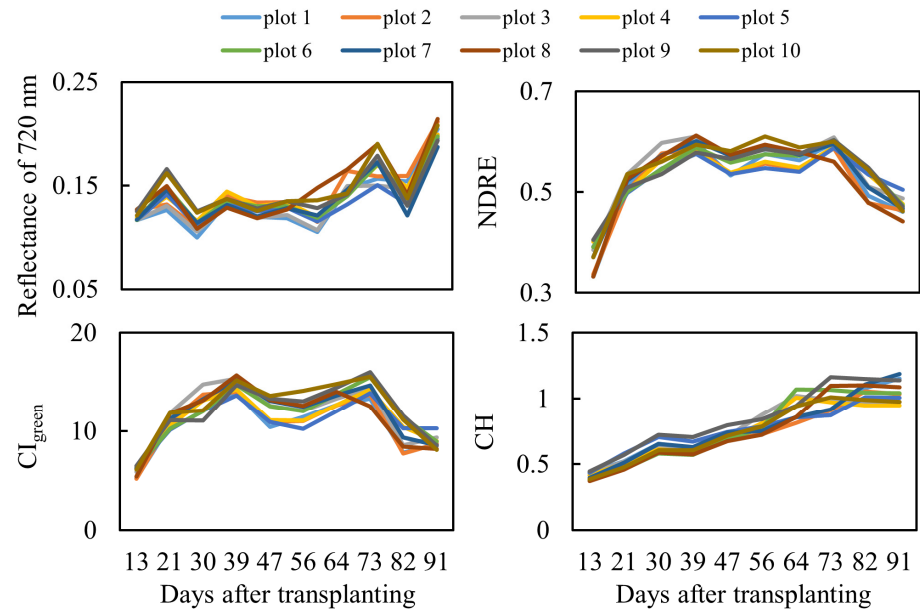


**Figure 6.** Time-series variation curves of canopy reflectance, VI, and CH in the selected plots.



**Figure 7.** Correlation of remote sensing variables with rice yield at different periods (\* indicates significant correlation at 0.05 confidence level).

The rice yield prediction models using NDRE, CH, and CV variables and multiple linear regression are shown in Figure 8. It can be observed that accurate rice yield prediction results cannot be obtained by directly utilizing remote sensing variables over multiple periods. The  $R^2$  of the models are all lower than 0.4, and the RMSE are all more than 1500 kg/ha. As can be seen from the normality test of the measured data, the yield data of the 289 plots conform to the standard normal distribution. The prediction results based on NDRE, CH, and CV show that there is an overestimation of rice yield in most of the plots, and the yield prediction values of the vast majority of the plots are greater than 9000 kg/ha. From the perspective of the distribution of yield, the results of yield prediction based on NDRE and CH show that there is a large number of clustering phenomena in the sample points, which cannot conform to the standard normal distribution. In the CV-based model, the phenomenon is modified. This shows the potential of CV to estimate rice yield with high accuracy.

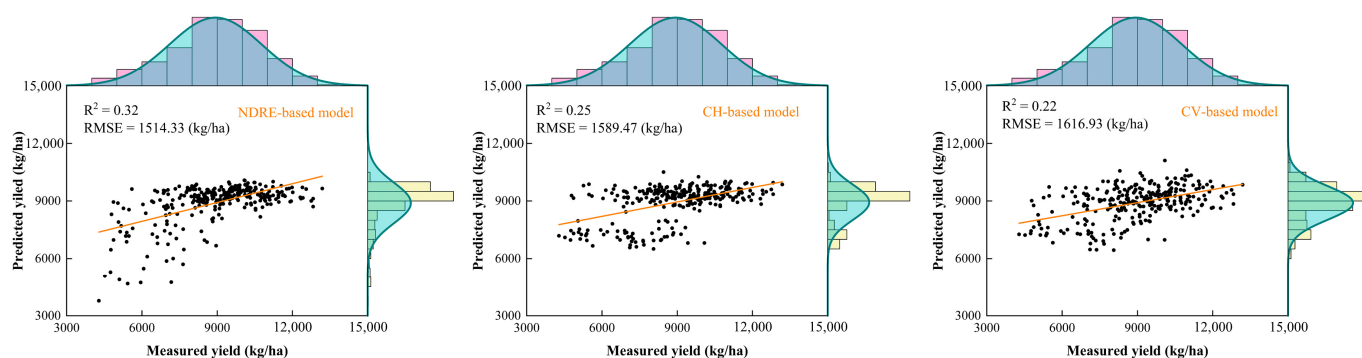


**Figure 8.** Comparison of rice yield estimation results based on multi-period NDRE, CH, and CV.

### 3.3. Rice Yield Prediction Based on Dynamic Process Clustering

#### 3.3.1. Clustering Based on Time-Series Reflectance Curves

To reduce the mutual impact among several sample groups, samples with similar curve trends were clustered. The k-shape technique was used to cluster the reflectance curves of various bands based on the SBD-based mass center calculation method. Figure 9 displays the results of using the corresponding variables from multiple periods to forecast the yield in each sample group. The prediction of rice yield is not significantly and consistently improved by clustering reflectance curves in any of the bands other than the red-edge bands (700 and 720 nm). The optimal rice yield prediction accuracy using this indicator is about 0.5 for  $R^2$  and about 1200 kg/ha for RMSE. The accuracy of estimating rice yield fluctuates irregularly as the number of clustering categories increases. In terms of local effects, the prediction accuracy of rice yield may show some improvement after realizing sample clustering. For instance, the accuracy  $R^2$  is increased by around 0.2, and the RMSE is decreased by roughly 600 kg/ha after using the 490 nm band reflectance curve to actualize the sample division of 5 and 8 categories. Following the sample division of two and four categories using the 800 nm band reflectance curve, the RMSE is decreased by about 800 kg/ha, and the accuracy  $R^2$  is increased by around 0.2. The accuracy  $R^2$  is increased by around 0.3, and the RMSE is decreased by more than 600 kg/ha after the 4- and 7-class sample division is realized using the 550 nm band reflectance curve. It goes without saying that improper clustering will reduce accuracy.

It was discovered that the accuracy of predicting rice yield considerably increased and stabilized after the samples were clustered using red-edge band reflectance curves. Clustering into six classes of samples improves the model accuracy the most when utilizing the 700 nm band. When compared to clustering into just two classes of samples, the  $R^2$  is increased by around 0.3, and the RMSE is decreased by roughly 700 kg/ha. The model's accuracy essentially remains the same as the number of clustering classes is increased. The model accuracy increased the most when using the 720 nm band and clustering into eight classes of samples. When only two classes of samples are clustered, the RMSE decreases by around 800 kg/ha, and the  $R^2$  improves by approximately 0.4. The accuracy of the model stops increasing as the clustering categories continue to grow. According to the aforementioned findings, rice growth may be described using red-edge band reflectance profiles.

#### 3.3.2. Clustering Based on Time-Series Vegetation Index Curves

Similar to the temporal reflectance curve clustering, different categories were clustered using the k-shape algorithm for different vegetation indices. In each category of samples, the rice yield was predicted using the corresponding variables in multiple periods, and the results are shown in Figure 10. It can be found that with the increase of clustering categories, the accuracy of rice yield estimation for different vegetation indices shows an

obvious and stable improvement. Except for the obvious accuracy improvement pattern, compared with the results of clustering using spectral curve features, the accuracy of rice yield prediction using vegetation index feature clustering is substantially improved, with the highest accuracy of  $R^2$  close to 0.8 and RMSE close to 400 kg/ha. With the increase in clustering categories, the accuracy of rice yield prediction firstly increases significantly and then basically remains stable. It is worth mentioning that when the highest rice yield prediction accuracy is obtained, the number of clustering categories characterized by different time-series vegetation index curves varies, and the number of categories maybe six, seven, or eight.

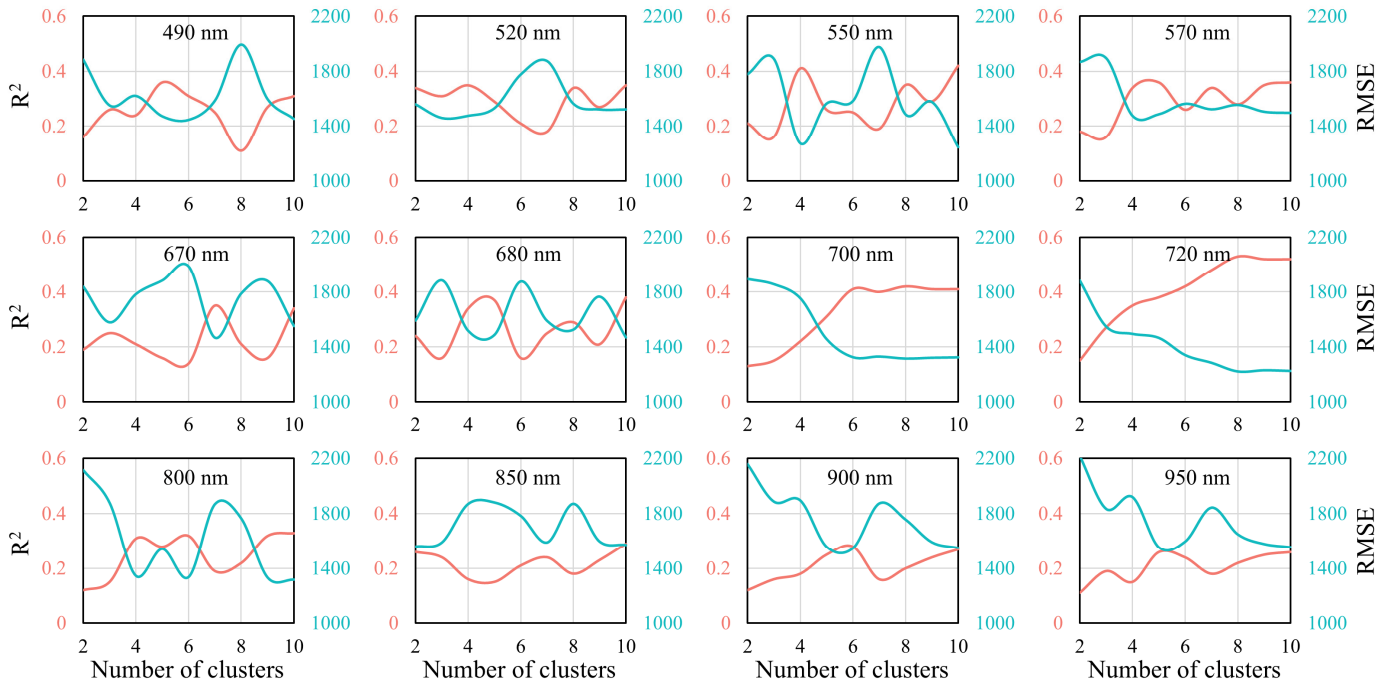


**Figure 9.** Trends in multi-period rice yield estimation results based on time-series feature clustering of reflectance curves in different bands.

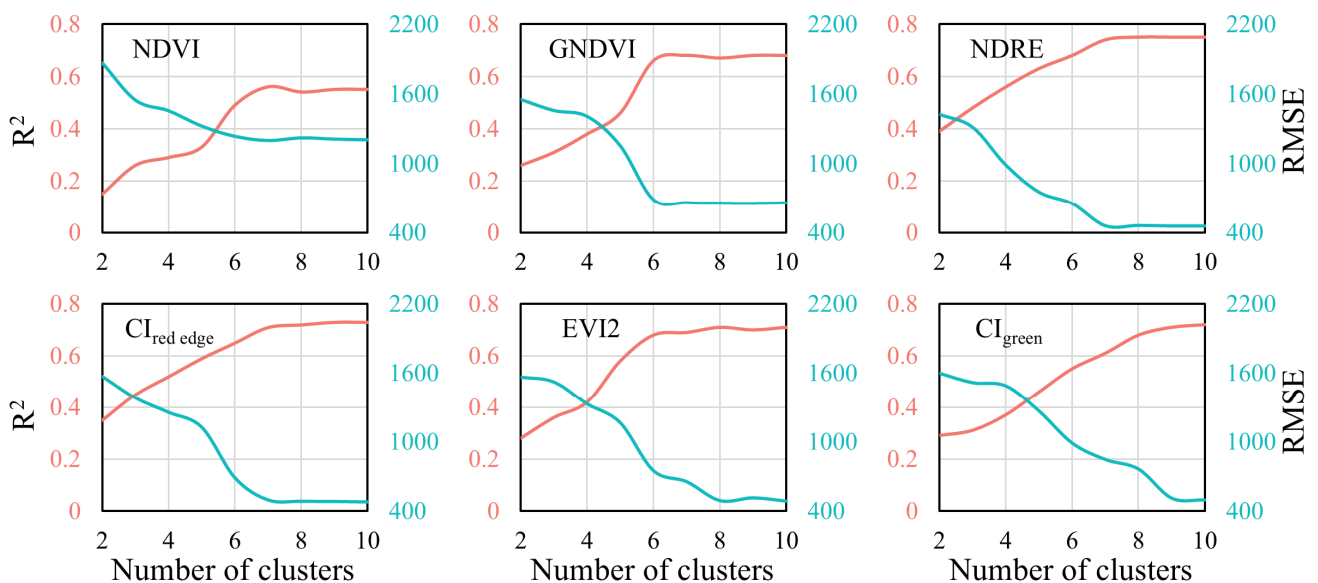


**Figure 10.** Trends in multi-period rice yield estimation results based on time-series vegetation indices curves clustering.

GNDVI only needs 289 samples to be clustered into six distinct groups, which is the smallest number of categories needed to achieve the best rice yield forecast accuracy. However,  $CI_{green}$  needs to be clustered into nine groups to attain the best estimation accuracy. When the NDVI is grouped into seven groups, the best accuracy is achieved. Nevertheless, there is room for improvement in the precision of rice yield estimation when compared to other vegetation indices. When estimating the yield using the NDVI curve, the highest accuracy  $R^2$  was less than 0.6, and the RMSE was greater than 1200 kg/ha. Based on the time-series curves of other vegetative indices, the maximum yield estimation accuracy  $R^2$  was approximately 0.7, with an RMSE of roughly 500 kg/ha. With an  $R^2$  of nearly 0.75, and an RMSE of roughly 400 kg/ha, the red-edge index curve-based estimation of rice yield exhibits the highest accuracy overall. Previous results have shown that the time-series features of vegetation indices, particularly red-edge indices, which have the greatest impact on rice yield estimation, can accurately describe the growth characteristics of rice over the entire period.

### 3.3.3. Clustering Based on Time-Series CH and CV Curves

Similar to the temporal reflectance curve and vegetation index curve clustering, different categories were clustered using the k-shape algorithm for CH and CV. In each category of samples, the corresponding variables of multiple periods were utilized to predict the yield, and the results are shown in Figure 11. It can be found that with the increase of clustering categories, the change rule of rice yield prediction accuracy based on CH and CV time-series curve characteristics shows a similar trend. The yield estimation accuracy reaches its highest when the number of clustering categories increases from two to six. When continuing to increase the clustering categories, the yield estimation accuracy remains stable. The  $R^2$  of the rice estimation model based on the clustering of CV temporal features is more than 0.8, and the RMSE is about 300 kg/ha. After utilizing the CH temporal curve to realize the division of the samples into two and six categories, the accuracy of  $R^2$  is increased by more than 0.4, and the RMSE is reduced by more than 1000 kg/ha. After utilizing the CV temporal curve to realize the division of the samples into two and six categories, the accuracy of  $R^2$  is increased by about 0.5, and the RMSE is reduced by more than 1200 kg/ha. The above results show that the CH and CV features of the time series can well characterize the growth of rice over the whole period. The accuracy of the rice yield estimation based on CV time-series curves was higher than that based on CH features. Rice yield estimation based on CH and CV time-series curves was more accurate than that based on reflectance and vegetation index characteristics.

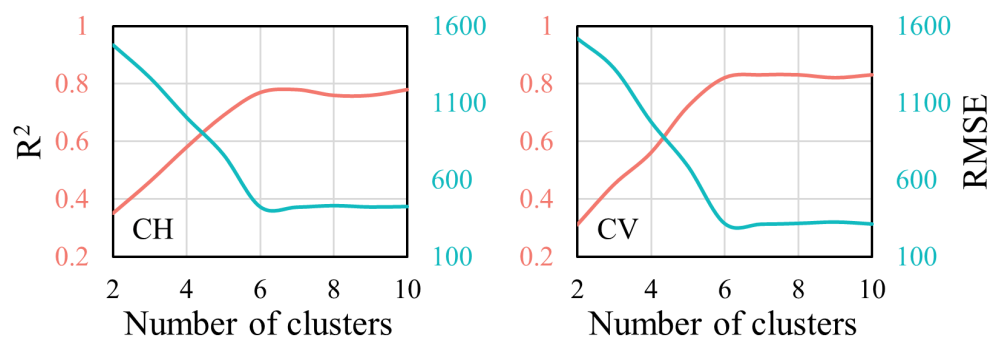


**Figure 11.** Trends in multi-period rice yield estimation results based on time-series CH and CV curve clustering.

Figure 12 displays the findings of the estimation of rice yield in Exp. 1 based on the numbers seven, six, and six for the NDRE, CH, and CV clustering groups, respectively. With an  $R^2$  of 0.82 and an RMSE of 315.39 kg/ha, it is evident that the rice yield estimation based

on CV temporal features has the highest accuracy. The accuracy of rice yield estimation based on NDRE and CH temporal features is somewhat worse. The model that is based on the clustering of NDRE time-series curve features has a lower RMSE of 1054.95 kg/ha and an improved  $R^2$  of 0.42 when compared to the accuracy of rice yield estimation using multi-period NDRE. The model that is based on the clustering of CH time-series curve features has a lower RMSE of 1165.79 kg/ha and an improved  $R^2$  of 0.52 when compared to the accuracy of rice yield estimation using multi-period CH. With a lowered RMSE of 1301.54 kg/ha and an improved  $R^2$  of 0.6, the model based on CV time-series curve feature clustering outperforms the accuracy of rice yield estimation using multi-period CV. From the distribution of predicted rice yield values, the results of yield prediction based on NDRE, CH, and CV time-series features all show a standard normal distribution, which is consistent with the distribution of measured values. This also indicates that the method shows excellent performance in both high- and low-yield value estimations without obvious overestimation and underestimation. When comparing the spectral and structural features, the accuracy of rice yield estimation based on CH and CV temporal features was 35.67 kg/ha and 143.96 kg/ha lower than the RMSE of the model accuracy based on NDRE temporal features, respectively. This demonstrates the prominent role of structural parameter growth features in rice yield estimation.

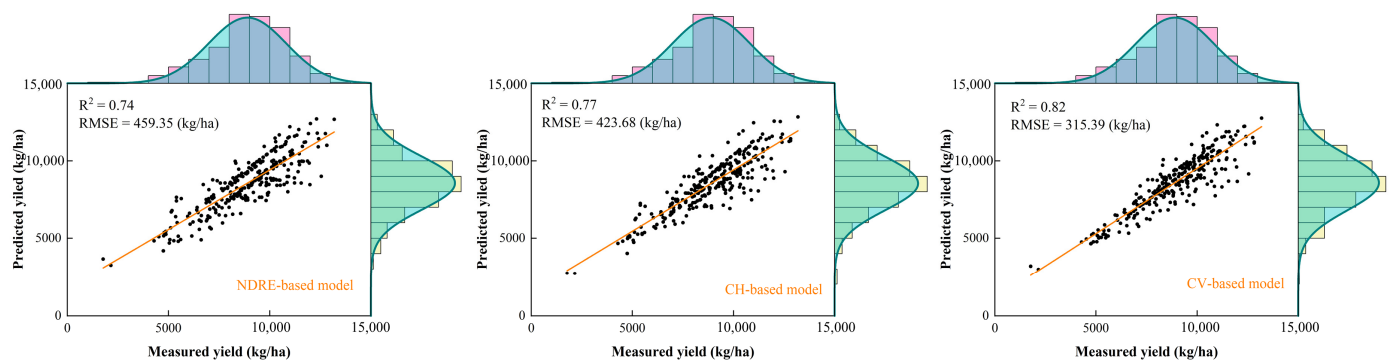


**Figure 12.** Comparison of rice yield estimation results based on clustering of the features of time-series curves of NDRE, CH, and CV in Exp. 1.

### 3.4. Validation of Rice Yield Prediction Models

Exp. 2 served as an independent validation set for the NDRE, CH, and CV temporal feature curve clustering models to confirm the benefits of the rice growth feature curve clustering method in yield prediction as well as the model's migratability. The outcomes are displayed in Figure 13. It is evident that the temporal curve feature clustering-based method performs well when calculating the multi-genotype rice yield. Similar to the findings of Exp. 1, the rice yield estimation model based on CV temporal characteristics achieves the best validation accuracy with  $R^2 = 0.85$ ,  $RMSE = 282.41$  kg/ha.  $R^2 = 0.82$ ,  $RMSE = 309.62$  kg/ha, and  $R^2 = 0.78$ ,  $RMSE = 463.69$  kg/ha are the results of the rice yield estimation model based on CH and NDRE temporal characteristics, respectively. The distribution of Exp. 2's measured yield data shows that the rice yield values follow a normal distribution. The distribution of the predicted rice values also matches a standard normal distribution. The conclusions show that the technique of using clustering of rice growth characteristic curves may successfully increase the precision of yield estimation in multi-genotype rice.

Like Exp. 2, the data obtained from Exp. 3 were used for independent validation, and the results are shown in Figure 13. Unlike Exp. 2, Exp. 3 contained fewer rice genotypes. However, Exp. 3 included more pronounced genotypic variability because one variety was Japonica rice. It can be seen that the method based on time-series remote sensing

feature clustering showed satisfactory accuracy. The order of rice yield prediction accuracy for different features remains consistent with that in Experiments 1 and 2. The results further demonstrate the feasibility of the proposed method for estimating rice yield in complex scenarios.

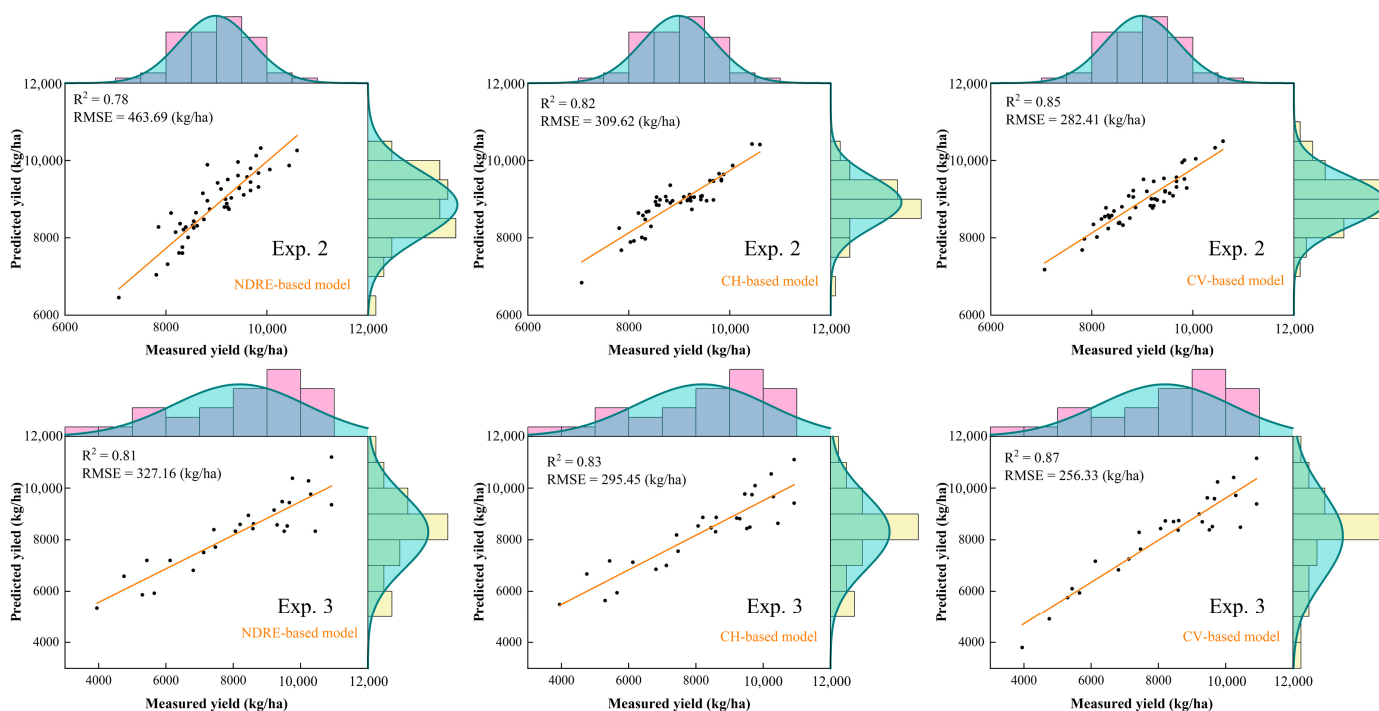


**Figure 13.** Comparison of rice yield estimation results based on multi-period NDRE, CH, and CV curve feature clustering in Exp. 2 and Exp. 3.

#### 4. Discussion

The formation of rice yield is a long-term accumulation process that is affected by multiple factors [34]. In remote sensing yield estimation, yield estimation models can be obtained based on a single growth stage, but the spectral information of multiple growth stages within a rice-growing season can more comprehensively reflect the yield formation process [7,35]. In this study, based on two years of independent field experiments with multiple genotypes of rice, the growth process of different genotypes of rice was characterized using growth characterization parameters, including vegetation index, canopy height, and canopy volume, based on the acquisition of RGB and multispectral images throughout the entire growth stage. The k-shape algorithm was applied to realize the clustering of rice genotypes with different similar growth characteristics. Ultimately, high-precision yield prediction of multi-genotype rice was achieved using multi-period remote sensing features. Compared with traditional yield prediction using spectral, vegetation index, or geometric features directly, the model has higher accuracy and stability.

Spectral information, especially vegetation indices, has long been recognized as a useful indicator of crop growth parameters and yield estimation [36,37]. For example, the leaf area index, chlorophyll content, and biomass of rice, wheat, and maize can be extracted with high accuracy using vegetation indices [38–40]. As different vegetation indices have been used for more refined studies, red-edge band-based vegetation indices are considered to have higher accuracy and more stable results in crop growth monitoring [41,42]. Red-edge indices have also shown better results than traditional vegetation indices for crop yield estimation [43,44]. Furthermore, some structural parameters such as canopy cover, canopy height, and canopy volume have been proposed to enhance crop growth parameters and

yield estimation [15]. Numerous studies have shown that in densely growing vegetation, structural parameters can compensate for the lack of spectral information and help improve the estimation of crop growth trait parameters [17,45,46].

In this study, it was found that the model accuracy was low when estimating rice yield using single-period vegetation indices and structural parameters. After combining the multi-period remote sensing indicators, the correlation with yield was significantly improved (Figure 7). Since remote sensing indicators in multiple periods carry different information on rice growth, and rice yield is the comprehensive result of biomass accumulation and distribution in various periods [5]. The expression for yield differences is facilitated by utilizing monitoring data at individual stages [18]. This demonstrates the importance of multi-period growth characteristics in the prediction of final rice yield. However, multi-species rice exhibits different growth characteristics when simulating rice cultivation under actual field conditions. As a result, the accuracy of yield estimation using a combination of multi-period vegetation indices remains poor (Figure 8). Direct comparisons of yield differences could not be made due to the variation in the growth cycles of different rice genotypes, resulting in the data observed not being within the same growth dimension. In this context, the accuracy of rice yield estimation based on multi-period remote sensing features was significantly improved after clustering the rice growth characteristics using a k-shape. The division of varieties with distinct growth characteristics enables the direct comparison of multiple variety yields within the same dimension. From Figure 9, we observe that the accuracy of rice yield estimation based on the red-edge band reflectance time-series curve features is significantly better than that using other band features. The results in Figure 10 indicate that the yield estimation models clustered with time-series characteristic curves of the red-edge indices (NDRE and  $CI_{red\ edge}$ ) have higher accuracy and stability compared to other vegetation indices. These findings further demonstrate the prominent role of the red-edged bands in rice yield estimation. The accuracy of rice yield estimation was further improved after utilizing CH and CV time-series curve feature clustering (Figure 11). Compared with the NDRE feature clustering model, the model based on structural feature clustering only needs to be clustered into six groups to obtain a higher and more stable model accuracy. It indicates that the temporal characteristics of structural parameters can better reflect the growth characteristics of different genotypes of rice. This conclusion is consistent with the findings of previous studies that used structural parameters to improve the accuracy of crop yield estimation [47].

In this study, the data obtained from Exp. 1 was utilized for ten-fold cross-validation, which resulted in a highly accurate estimation model. On this basis, Exp. 2 was used for independent validation. The results show that the estimation accuracy in Exp. 2 is higher than the model accuracy in Exp. 1 based on the corresponding NDRE, CH, and CV temporal feature models. It also shows that the accuracy of the model proposed in this study is affected by the number of samples. Exp. 2 contained 48 different rice varieties, which was significantly lower than the 289 samples in Exp. 1. This also indirectly indicates that the complexity of the growth characteristics of the different genotypes of rice in Exp. 2 is lower than that of rice in Exp. 1. From the clustering of different remote sensing indicators, it can be observed that there are differences in the number of growth feature clusters of different complexities when obtaining the highest rice yield estimation accuracy. For example, the yield estimation accuracy based on spectral reflectance curve feature clustering is unstable. The number of categories based on vegetation index curve feature clustering is large. This is most likely due to the fact that spectral information is susceptible to light variations and canopy structure, which results in overly complex curve features [48,49]. The extracted rice structural features are less affected by factors such as light; therefore, a more stable model accuracy can be obtained. This can also be verified in Exp. 3.

In the next step of this study, more variables that can effectively characterize the rice growth process will be explored. Meanwhile, the factors affecting the growth characteristics of rice will be emphasized. Examples include the growth stage, field management practices, planting density, and variety type. Based on this, additional genotype clustering methods that can be interpreted will be developed. Additionally, we will study exactly which periods have an impact on final yield as a way to simplify the data acquisition cycle.

The object of this study is plot-scale multi-genotype rice. Experiments and validation have not been conducted in other scenarios, such as nitrogen gradient, stress environments, different planting densities, and cropping styles. In existing yield estimation studies, linear regression models are mainly used for a single variety as well as for nitrogen fertilizer control experimental scenarios [17]. Machine learning and deep learning models are mostly used for multi-genotype crop yield estimations [22,50]. Studies similar to the present study on estimating yield after automatic classification of multiple rice genotypes have not been reported.

## 5. Conclusions

In this study, a high-precision prediction method for multi-genotype rice based on time-series remote sensing images and dynamic growth process clustering was proposed. The structural and spectral information of the rice canopy, including CH, CV, and some vegetation indices, were extracted for the whole period using RGB and multispectral images, respectively. The time-series reflectance, VIs, CH, and CV curves were used as representatives of the rice growth process to cluster multi-genotype rice. The results showed that the red-edge bands were superior to the other bands in clustering the reflectance time-series curves for yield estimation. When estimating rice yield using VIs time-series curve feature clustering, the accuracy of rice yield estimation was substantially improved compared to the reflectance model, especially when using red-edge indices. When using CH and CV time-series feature clustering for rice yield estimation, the model accuracy was further improved, and the predicted yield distribution conformed to the standard normal distribution, as did the measured data, demonstrating that it can be well adapted to the prediction of both high- and low-value rice yield. The rice yield estimation based on CV temporal features had the highest accuracy with an  $R^2$  of 0.82 and RMSE of 315.39 kg/ha. The proposed method can effectively solve the problem of low-yield estimation accuracy of multi-genotype rice and assist in fine management under natural rice-growing conditions.

**Author Contributions:** Conceptualization, methodology, writing—original draft preparation, Q.L.; software, validation, data curation, S.Z. and L.D. writing—review and editing, S.L. All authors have read and agreed to the published version of the manuscript.

**Funding:** This research was funded by the Joint Fund of Henan Province Science and Technology R&D Program, grant number 235200810069; the Science and Technology Tackling Project of Henan Province, grant number 242102210011; the Basic Research Operating Expenses Program of Henan Academy of Sciences, grant number 240625002; and the Scientific Research Initiation Program for High-level Talents of Henan Academy of Sciences, grants numbers 241825015 and 241824205.

**Institutional Review Board Statement:** Not applicable.

**Data Availability Statement:** Related data are available upon reasonable request.

**Conflicts of Interest:** The authors declare no conflicts of interest.

## References

- Sagart, L. How Many Independent Rice Vocabularies in Asia? *Rice* **2011**, *4*, 121–133. [[CrossRef](#)]
- Satoh, R.; Tsuge, I.; Tokuda, R.; Teshima, R. Analysis of the distribution of rice allergens in brown rice grains and of the allergenicity of products containing rice bran. *Food Chem.* **2019**, *276*, 761–767. [[CrossRef](#)]
- Liao, C.J.; Fang, S.L.; Zhang, H.D.; Liu, L.S.; Xie, J.X.; Li, X.; Cao, F.B.; Chen, J.N.; Huang, M. Grain Yield and Yield Attributes of Currently Popular Hybrid Rice Varieties Compared to Representative Super Hybrid Rice Varieties in Subtropical Environments. *Agronomy* **2024**, *14*, 11. [[CrossRef](#)]
- Xue, H.Y.; Xu, X.G.; Zhu, Q.Z.; Meng, Y.; Long, H.L.; Li, H.L.; Song, X.Y.; Yang, G.J.; Yang, M.; Li, Y.F.; et al. Rice yield and quality estimation coupling hierarchical linear model with remote sensing. *Comput. Electron. Agric.* **2024**, *218*, 12. [[CrossRef](#)]
- dela Torre, D.M.G.; Gao, J.; Macinnis-Ng, C. Remote sensing-based estimation of rice yields using various models: A critical review. *Geo-Spat. Inf. Sci.* **2021**, *24*, 580–603. [[CrossRef](#)]
- Wang, F.L.; Wang, F.M.; Zhang, Y.; Hu, J.H.; Huang, J.F.; Xie, J.K. Rice Yield Estimation Using Parcel-Level Relative Spectra Variables From UAV-Based Hyperspectral Imagery. *Front. Plant Sci.* **2019**, *10*, 12. [[CrossRef](#)]
- Yang, Q.; Shi, L.S.; Han, J.Y.; Zha, Y.Y.; Zhu, P.H. Deep convolutional neural networks for rice grain yield estimation at the ripening stage using UAV-based remotely sensed images. *Field Crop. Res.* **2019**, *235*, 142–153. [[CrossRef](#)]
- Wang, F.M.; Yao, X.P.; Xie, L.L.; Zheng, J.Y.; Xu, T.Y. Rice Yield Estimation Based on Vegetation Index and Florescence Spectral Information from UAV Hyperspectral Remote Sensing. *Remote Sens.* **2021**, *13*, 19. [[CrossRef](#)]
- Franch, B.; San Bautista, A.; Fita, D.; Rubio, C.; Tarrazó-Serrano, D.; Sánchez, A.; Skakun, S.; Vermote, E.; Becker-Reshef, I.; Uris, A. Within-Field Rice Yield Estimation Based on Sentinel-2 Satellite Data. *Remote Sens.* **2021**, *13*, 22. [[CrossRef](#)]
- Soriano-González, J.; Angelats, E.; Martínez-Eixarch, M.; Alcaraz, C. Monitoring rice crop and yield estimation with Sentinel-2 data. *Field Crop. Res.* **2022**, *281*, 11. [[CrossRef](#)]
- Yang, Q.; Shi, L.S.; Han, J.Y.; Chen, Z.W.; Yu, J. A VI-based phenology adaptation approach for rice crop monitoring using UAV multispectral images. *Field Crop. Res.* **2022**, *277*, 13. [[CrossRef](#)]
- Xu, S.Z.; Xu, X.A.; Zhu, Q.Z.; Meng, Y.; Yang, G.J.; Feng, H.K.; Yang, M.; Zhu, Q.L.; Xue, H.Y.; Wang, B.B. Monitoring leaf nitrogen content in rice based on information fusion of multi-sensor imagery from UAV. *Precis. Agric.* **2023**, *24*, 2327–2349. [[CrossRef](#)]
- Li, B.; Xu, X.M.; Zhang, L.; Han, J.W.; Bian, C.S.; Li, G.C.; Liu, J.G.; Jin, L.P. Above-ground biomass estimation and yield prediction in potato by using UAV-based RGB and hyperspectral imaging. *ISPRS-J. Photogramm. Remote Sens.* **2020**, *162*, 161–172. [[CrossRef](#)]
- Maimaitijiang, M.; Sagan, V.; Sidike, P.; Hartling, S.; Esposito, F.; Fritschi, F.B. Soybean yield prediction from UAV using multimodal data fusion and deep learning. *Remote Sens. Environ.* **2020**, *237*, 20. [[CrossRef](#)]
- Ashapure, A.; Jung, J.H.; Chang, A.J.; Oh, S.; Yeom, J.; Maeda, M.; Maeda, A.; Dube, N.; Landivar, J.; Hague, S.; et al. Developing a machine learning based cotton yield estimation framework using multi-temporal UAS data. *ISPRS-J. Photogramm. Remote Sens.* **2020**, *169*, 180–194. [[CrossRef](#)]
- Xu, L.; Ming, D.P.; Du, T.Y.; Chen, Y.Y.; Dong, D.H.; Zhou, C.H. Delineation of cultivated land parcels based on deep convolutional networks and geographical thematic scene division of remotely sensed images. *Comput. Electron. Agric.* **2022**, *192*, 16. [[CrossRef](#)]
- Feng, A.J.; Zhou, J.F.; Vories, E.D.; Sudduth, K.A.; Zhang, M.N. Yield estimation in cotton using UAV-based multi-sensor imagery. *Biosyst. Eng.* **2020**, *193*, 101–114. [[CrossRef](#)]
- Zhou, X.; Zheng, H.B.; Xu, X.Q.; He, J.Y.; Ge, X.K.; Yao, X.; Cheng, T.; Zhu, Y.; Cao, W.X.; Tian, Y.C. Predicting grain yield in rice using multi-temporal vegetation indices from UAV-based multispectral and digital imagery. *ISPRS-J. Photogramm. Remote Sens.* **2017**, *130*, 246–255. [[CrossRef](#)]
- Marcone, A.; Impollonia, G.; Croci, M.; Blandinières, H.; Pellegrini, N.; Amaducci, S. Garlic yield monitoring using vegetation indices and texture features derived from UAV multispectral imagery. *Smart Agric. Technol.* **2024**, *8*, 13. [[CrossRef](#)]
- Yuan, J.H.; Zhang, Y.L.; Zheng, Z.J.; Yao, W.; Wang, W.S.; Guo, L.F. Grain Crop Yield Prediction Using Machine Learning Based on UAV Remote Sensing: A Systematic Literature Review. *Drones* **2024**, *8*, 27. [[CrossRef](#)]
- Fan, J.H.; Zhou, J.; Wang, B.W.; de Leon, N.; Kaeppler, S.M.; Lima, D.C.; Zhang, Z. Estimation of Maize Yield and Flowering Time Using Multi-Temporal UAV-Based Hyperspectral Data. *Remote Sens.* **2022**, *14*, 16. [[CrossRef](#)]
- Shi, G.W.; Du, X.; Du, M.W.; Li, Q.Z.; Tian, X.L.; Ren, Y.T.; Zhang, Y.; Wang, H.Y. Cotton Yield Estimation Using the Remotely Sensed Cotton Boll Index from UAV Images. *Drones* **2022**, *6*, 23. [[CrossRef](#)]
- Zhang, C.S.; Diao, C.Y. A Phenology-guided Bayesian-CNN (PB-CNN) framework for soybean yield estimation and uncertainty analysis. *ISPRS-J. Photogramm. Remote Sens.* **2023**, *205*, 50–73. [[CrossRef](#)]
- Pei, J.; Tan, S.F.; Zou, Y.P.; Liao, C.H.; He, Y.N.; Wang, J.; Huang, H.B.; Wang, T.X.; Tian, H.F.; Fang, H.J.; et al. The role of phenology in crop yield prediction: Comparison of ground-based phenology and remotely sensed phenology. *Agric. For. Meteorol.* **2025**, *361*, 14. [[CrossRef](#)]
- Zhou, M.; Zheng, H.B.; He, C.; Liu, P.; Awan, G.M.; Wang, X.; Cheng, T.; Zhu, Y.; Cao, W.X.; Yao, X. Wheat phenology detection with the methodology of classification based on the time-series UAV images. *Field Crop. Res.* **2023**, *292*, 12. [[CrossRef](#)]

26. Martinez-Tejada, I.; Riedel, C.S.; Juhler, M.; Andresen, M.; Wilhjelm, J.E. k-Shape clustering for extracting macro-patterns in intracranial pressure signals. *Fluids Barriers CNS* **2022**, *19*, 13. [[CrossRef](#)] [[PubMed](#)]
27. Rouse, J.W. Monitoring the vernal advancement and retrogradation (greenwave effect) of natural vegetation. In *Technical Report, Progress Report RSC 1978-2 for NASA, Greenbelt, USA*; NASA: Washington, DC, USA, 1974.
28. Gitelson, A.A.; Merzlyak, M.N. Signature analysis of leaf reflectance spectra: Algorithm development for remote sensing of chlorophyll. *J. Plant Physiol.* **1996**, *148*, 494–500. [[CrossRef](#)]
29. Fitzgerald, G.J.; Rodriguez, D.; Christensen, L.K.; Belford, R.; Sadras, V.O.; Clarke, T.R. Spectral and thermal sensing for nitrogen and water status in rainfed and irrigated wheat environments. *Precis. Agric.* **2006**, *7*, 233–248. [[CrossRef](#)]
30. Gitelson, A.A.; Gritz, Y.; Merzlyak, M.N. Relationships between leaf chlorophyll content and spectral reflectance and algorithms for non-destructive chlorophyll assessment in higher plant leaves. *J. Plant Physiol.* **2003**, *160*, 271–282. [[CrossRef](#)] [[PubMed](#)]
31. Jiang, Z.Y.; Huete, A.R.; Didan, K.; Miura, T. Development of a two-band enhanced vegetation index without a blue band. *Remote Sens. Environ.* **2008**, *112*, 3833–3845. [[CrossRef](#)]
32. Gitelson, A.A.; Keydan, G.P.; Merzlyak, M.N. Three-band model for noninvasive estimation of chlorophyll, carotenoids, and anthocyanin contents in higher plant leaves. *Geophys. Res. Lett.* **2006**, *33*, 5. [[CrossRef](#)]
33. Wang, X.; Song, R.B.; Xiao, J.M.; Li, T.; Li, X.Q. Accelerating k-Shape Time Series Clustering Algorithm Using GPU. *IEEE Trans. Parallel Distrib. Syst.* **2023**, *34*, 2718–2734. [[CrossRef](#)]
34. Wang, F.M.; Wang, F.L.; Hu, J.H.; Xie, L.L.; Yao, X.P. Rice Yield Estimation Based on an NPP Model With a Changing Harvest Index. *IEEE J. Sel. Top. Appl. Earth Observ. Remote Sens.* **2020**, *13*, 2953–2959. [[CrossRef](#)]
35. Yang, R.; Zhou, J.; Lu, X.Y.; Shen, J.X.; Chen, H.Z.; Chen, M.Y.; He, Y.; Liu, F. A robust rice yield estimation framework developed by grading modeling and normalized weight decision-making strategy using UAV imaging technology. *Comput. Electron. Agric.* **2023**, *215*, 13. [[CrossRef](#)]
36. Wang, Z.L.; Tan, X.M.; Ma, Y.M.; Liu, T.; He, L.M.; Yang, F.; Shu, C.H.; Li, L.L.; Fu, H.; Li, B.; et al. Combining canopy spectral reflectance and RGB images to estimate leaf chlorophyll content and grain yield in rice. *Comput. Electron. Agric.* **2024**, *221*, 15. [[CrossRef](#)]
37. Guo, Y.H.; Wang, H.X.; Wu, Z.F.; Wang, S.X.; Sun, H.Y.; Senthilnath, J.; Wang, J.Z.; Bryant, C.R.; Fu, Y.S. Modified Red Blue Vegetation Index for Chlorophyll Estimation and Yield Prediction of Maize from Visible Images Captured by UAV. *Sensors* **2020**, *20*, 16. [[CrossRef](#)] [[PubMed](#)]
38. Li, S.Y.; Yuan, F.; Ata-Ul-Karim, S.T.; Zheng, H.B.; Cheng, T.; Liu, X.J.; Tian, Y.C.; Zhu, Y.; Cao, W.X.; Cao, Q. Combining Color Indices and Textures of UAV-Based Digital Imagery for Rice LAI Estimation. *Remote Sens.* **2019**, *11*, 21. [[CrossRef](#)]
39. Wang, A.C.; Song, Z.S.; Xie, Y.W.; Hu, J.; Zhang, L.Y.; Zhu, Q.Z. Detection of Rice Leaf SPAD and Blast Disease Using Integrated Aerial and Ground Multiscale Canopy Reflectance Spectroscopy. *Agriculture* **2024**, *14*, 19. [[CrossRef](#)]
40. Li, F.; Piasecki, C.; Millwood, R.J.; Wolfe, B.; Mazarei, M.; Stewart, C.N. High-Throughput Switchgrass Phenotyping and Biomass Modeling by UAV. *Front. Plant Sci.* **2020**, *11*, 15. [[CrossRef](#)] [[PubMed](#)]
41. Qiao, L.; Zhao, R.M.; Tang, W.J.; An, L.L.; Sun, H.; Li, M.Z.; Wang, N.; Liu, Y.; Liu, G.H. Estimating maize LAI by exploring deep features of vegetation index map from UAV multispectral images. *Field Crop. Res.* **2022**, *289*, 14. [[CrossRef](#)]
42. Cheng, J.P.; Yang, H.; Qi, J.B.; Sun, Z.D.; Han, S.Y.; Feng, H.K.; Jiang, J.Y.; Xu, W.M.; Li, Z.H.; Yang, G.J.; et al. Estimating canopy-scale chlorophyll content in apple orchards using a 3D radiative transfer model and UAV multispectral imagery. *Comput. Electron. Agric.* **2022**, *202*, 15. [[CrossRef](#)]
43. Ali, N.; Mohammed, A.; Bais, A.; Berraies, S.; Ruan, Y.F.; Cuthbert, R.D.; Sangha, J.S. Field-Scale Precision: Predicting Grain Yield of Diverse Wheat Breeding Lines Using High-Throughput UAV Multispectral Imaging. *IEEE J. Sel. Top. Appl. Earth Observ. Remote Sens.* **2024**, *17*, 11419–11433. [[CrossRef](#)]
44. Camenzind, M.P.; Yu, K. Multi temporal multispectral UAV remote sensing allows for yield assessment across European wheat varieties already before flowering. *Front. Plant Sci.* **2024**, *14*, 19. [[CrossRef](#)]
45. Yu, D.Y.; Zha, Y.Y.; Shi, L.S.; Jin, X.L.; Hu, S.; Yang, Q.; Huang, K.; Zeng, W.Z. Improvement of sugarcane yield estimation by assimilating UAV-derived plant height observations. *Eur. J. Agron.* **2020**, *121*, 16. [[CrossRef](#)]
46. Liu, T.; Wu, F.; Mou, N.N.; Zhu, S.L.; Yang, T.L.; Zhang, W.J.; Wang, H.; Wu, W.; Zhao, Y.Y.; Sun, C.M.; et al. The estimation of wheat yield combined with UAV canopy spectral and volumetric data. *Food Energy Secur.* **2024**, *13*, 17. [[CrossRef](#)]
47. Zhou, W.Q.; Song, C.; Liu, C.L.; Fu, Q.; An, T.H.; Wang, Y.J.; Sun, X.B.; Wen, N.; Tang, H.; Wang, Q. A Prediction Model of Maize Field Yield Based on the Fusion of Multitemporal and Multimodal UAV Data: A Case Study in Northeast China. *Remote Sens.* **2023**, *15*, 22. [[CrossRef](#)]
48. Luo, S.J.; Jiang, X.Q.; Yang, K.L.; Li, Y.J.; Fang, S.H. Multispectral remote sensing for accurate acquisition of rice phenotypes: Impacts of radiometric calibration and unmanned aerial vehicle flying altitudes. *Front. Plant Sci.* **2022**, *13*, 19. [[CrossRef](#)] [[PubMed](#)]

49. Muramatsu, K.; Yoneda, E.; Soyama, N.; Thanyapraneedkul, J.; López-Ballesteros, A. Use of light response curve parameters to estimate gross primary production capacity from chlorophyll indices of global observation satellite and flux data. *Sci. Remote Sensing* **2024**, *10*, 16. [[CrossRef](#)]
50. Li, D.H.; Sun, X.X.; Jia, Y.H.; Yao, Z.W.; Lin, P.Y.; Chen, Y.Y.; Zhou, H.B.; Zhou, Z.Q.; Wu, K.X.; Shi, L.L.; et al. A longan yield estimation approach based on UAV images and deep learning. *Front. Plant Sci.* **2023**, *14*, 17. [[CrossRef](#)]

**Disclaimer/Publisher's Note:** The statements, opinions and data contained in all publications are solely those of the individual author(s) and contributor(s) and not of MDPI and/or the editor(s). MDPI and/or the editor(s) disclaim responsibility for any injury to people or property resulting from any ideas, methods, instructions or products referred to in the content.